Molecular Crystals and Liquid Crystals Science and Technology. Section A. Molecular Crystals and Liquid Crystals
Publication details, including instructions for authors and subscription information:
http://www.tandfonline.com/loi/gmcl19

A Novel Optical Method for Monitoring Homeotropic Alignment, Applied to a Side Chain Liquid Crystal Polymer in AC and DC Electric Fields

R. B. Findlay [a] & A. H. Windle [a]
[a] Department of Materials Science and Metallurgy, University of Cambridge, Pembroke Street, Cambridge, CB2 3QZ, United Kingdom
Version of record first published: 24 Sep 2006.

To cite this article: R. B. Findlay & A. H. Windle (1994): A Novel Optical Method for Monitoring Homeotropic Alignment, Applied to a Side Chain Liquid Crystal Polymer in AC and DC Electric Fields, Molecular Crystals and Liquid Crystals Science and Technology. Section A. Molecular Crystals and Liquid Crystals, 241:1, 255-273

To link to this article: http://dx.doi.org/10.1080/10587259408029763

Mol. Cryst. Liq. Cryst., 1994, Vol. 241, pp. 255–273
Reprints available directly from the publisher
Photocopying permitted by license only

Printed in the United States of America

A Novel Optical Method for Monitoring Homeotropic Alignment, Applied to a Side Chain Liquid Crystal Polymer in AC and DC Electric Fields

R. B. FINDLAY and A. H. WINDLE†

Department of Materials Science and Metallurgy, University of Cambridge, Pembroke Street, Cambridge CB2 3QZ, United Kingdom

(Received April 3, 1992; in final form August 20, 1993)

A novel, low-cost method is developed to study the kinetics of homeotropic alignment in uniaxial materials. The technique is evaluated relative to existing methods and calibrated against conoscopy. The kinetics of alignment of poly(MO6ONS) in alternating electric fields are studied, using the novel method, while the sample cools from the isotropic to the smectic phase. The dependence on sample thickness, field strength and cooling rate are examined. These results, together with differential scanning calorimetry (DSC) and optical clarity studies, are used to investigate the nature of the isotropic-smectic phase transition. The orientation and conductivity of a side chain liquid crystalline polymer are monitored while the sample is cooled in d.c. electric fields. Different effects are seen for a.c. and d.c. fields, particularly at temperatures just above the isotropic-smectic transition. A mechanism for the effects is proposed and related to the molecular structure of the material.

Keywords: homeotropic alignment, side chain liquid crystalline polymer, optical analysis

INTRODUCTION

Much optical analysis work involves nothing more sophisticated than a photodiode stuck to the eyepiece of a microscope, while the sample undergoes field and/or heat treatments between crossed or parallel polars.[1–12] This method is commonly used to generate an electronic signal so that the rate of a given optical effect can be measured automatically, or to measure the temperature of a phase transition as an alternative or supplement to DSC.

There is an interesting variation on this technique in which the light is still transmitted normal to the sample, but the tilt of the director relative to the light path is continuously variable, giving rise to interference fringes as the birefringence develops.[13–17] This method allows the alignment to be measured against voltage, time or temperature, so long as the sample is sufficiently transparent.

†To whom correspondence should be addressed.

These techniques are of limited value with uniaxial materials when the alignment is homeotropic, as no birefringence is then seen by light transmitted normal to the sample. To study the development of homeotropic alignment, either the whole conoscopic image must be monitored (which is possible with hot samples using objective lenses with high numerical apertures and long working distances), an anisotropic dye must be added (at the risk of altering the properties of the system), or the sample must be tilted off-axis and the polars set at 45° to the plane of tilt (as in the present technique).

It is remarkable how few workers have used these optical techniques in the study of smectic alignment. One reason is that smectic textures commonly scatter light, which makes analysis of the results complicated. Most workers prefer to use more direct measurements such as those from nuclear magnetic resonance (NMR) and dielectric relaxation spectroscopy (DRS). A great advantage of optical methods is that they are relatively easy to use and yield results quickly with simple and inexpensive apparatus, although quantitative analysis of the results can be difficult.

Electric and magnetic fields can be used to align side chain liquid crystalline materials,[8,18–20] especially to improve the nonlinear optical properties.[21,22] Most work has concentrated on nematics, but alternating electric field alignment of smectic A has also been demonstrated.[2,23–25]

Electrohydrodynamic instability is a problem encountered when poling liquid materials. There are several types of instability,[26] of which some are isotropic modes, which can occur in any liquid (including anisotropic ones) and are caused by charge injection, and others are anisotropic modes, which can occur only in anisotropic liquids such as liquid crystals. In d.c. poling, charge movement would risk breakdown and any instabilities would cause scattering and reduce the poling efficiency, so poling is usually performed at around the glass transition temperature where backbone motion is restricted. Some alignment, possibly due to shear flow caused by instabilities, has been seen using d.c. fields in the liquid crystalline phase of some materials.[27]

The material studied here is one of a range[28] synthesised at Hoechst-Celanese in Summit, New Jersey, USA, and is a homopolymer referred to as poly(MO6ONS). The side group is nitrostilbene, connected to a methacrylate backbone by an alkyl spacer of length 6. Its successful alignment in both alternating electric fields and surface fields has already been reported, and the resulting microstructure characterised.[29]

EXPERIMENTAL METHOD

The conoscopic image of an optically anisotropic sample reveals much about the orientation and crystal structure of the material; it is like part of a stereogram mapping the appearance of the sample when viewed from different orientations between crossed polars. Recording the conoscopic image using a video camera, and analysing it by computer, would therefore be a good way to monitor the development of alignment. This would require a microscope objective lens with a large numerical aperture and a long working distance to separate it from the hot

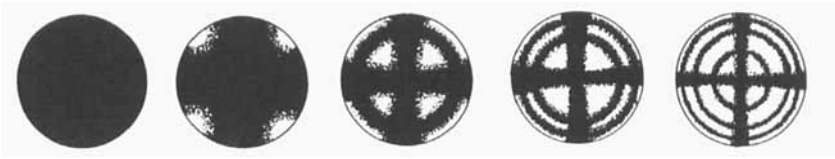

FIGURE 1 Idealised development of the conoscopic image during the transition from the isotropic phase to a transparent, homeotropically aligned monodomain (left to right).

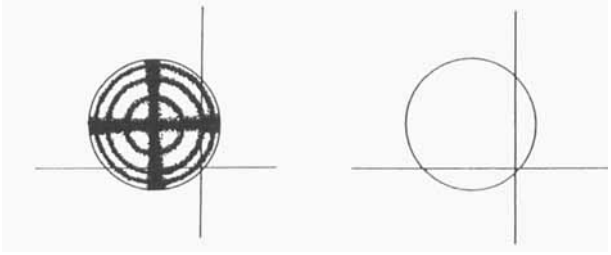

FIGURE 2 The crosshair indicates the point at which the light intensity is measured by the apparatus (shown here for Figure 1). Left: between crossed polars. Right: without analyser.

sample. These are now available, although the objective lenses are expensive and there may be problems with achieving good convergent illumination through a hotstage.

The present polymer is smectic A; it has positive dielectric anisotropy, and therefore aligns in high-frequency electric fields to form a uniaxial, homeotropic texture.[29] The conoscopic image has high symmetry, and the only changing features in monochromatic light are the positions of the interference rings, which move inwards as the degree of alignment, and thus the birefringence, increases (see Figure 1). Therefore we do not need to observe the entire conoscopic image; it is possible to characterise the development of orientation by measuring the intensity of the figure at one point in one of the quadrants (see Figure 2). This interference intensity will be zero for an isotropic sample and increase as the sample aligns, dipping every time an interference ring moves past that position on the conoscopic image. The birefringence is then proportional to the number of peaks and troughs in the interference intensity curve.

The apparatus is illustrated in Figure 3. The sample rests on a Linkam THM600 hotstage fitted with an angled top, and controlled by a Linkam TMS90 controller. A double window (not shown) is placed on top of the sample to improve thermal control.

Laser light passes through a polariser which is set at 45° to the plane of the diagram. It then passes through the sample to the analyser (another polariser crossed with respect to the first polariser), and its intensity (the *recorded interference intensity*) is measured using a photodiode.

There is a beamsplitter before the analyser, so that the intensity of transmitted light (the *clarity*) can be measured. Dividing the recorded interference intensity by the clarity gives the *normalised interference intensity*, corrected for the effects of light scattering. The beamsplitter is a glass slide coated with aluminium, with the metallised surface facing the incoming beam so as to avoid polarisation effects

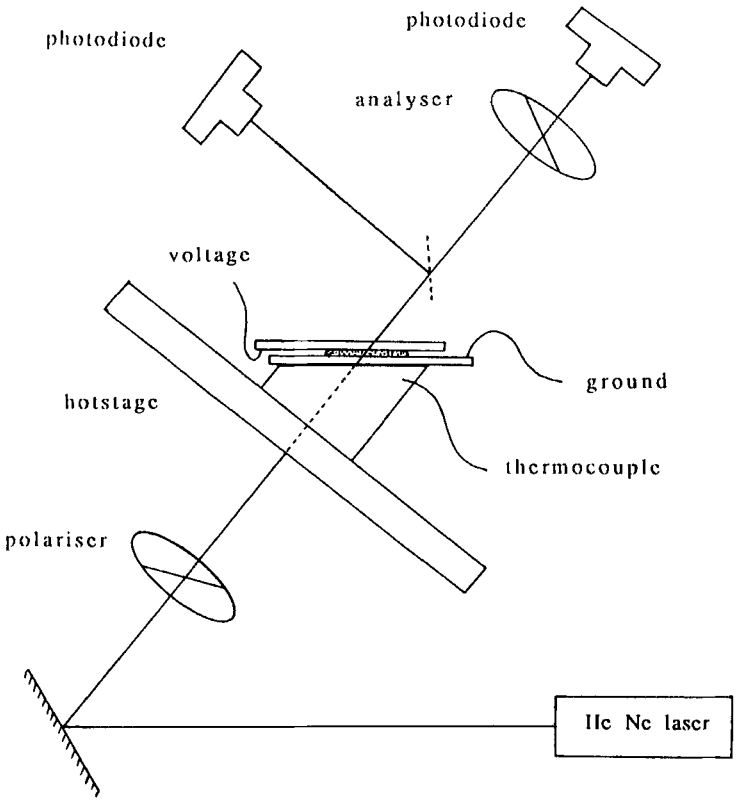

FIGURE 3 Experimental apparatus.

caused by reflection from the surface of a dielectric. There will, however, be some polarisation effects due to reflection from the glass in the sample assembly, which may cause small interference effects in the clarity curve.

A thermocouple is placed close to the sample inside the angled hotstage top, allowing accurate relative temperature measurements to be made, although absolute temperature readings are unreliable. Data from the thermocouple and photodiodes are collected by a computer. The preparation of the parallel-sided melt-pressed samples has previously been described,[29] and it is found that good alignment only occurs where the sample flowed between the slides, producing some backbone alignment. All voltages are quoted as peak-peak values.

If the sample always aligned to form a perfectly transparent monodomain, then the experimental results would be similar to those drawn in Figure 4, the intensity of the conoscopic image being measured at the point shown in Figure 2. In the isotropic phase, the sample is in extinction when viewed from all positions (between crossed polars), so the recorded interference intensity is zero (compare with Figure 1a). For this illustration, the rate of increase of birefringence is assumed to be constant with temperature through the transition, producing sinusoidal fringes at equal temperature intervals (as in Figure 1b–d). When the sample is all in the smectic phase, the recorded interference intensity is assumed to stop changing.

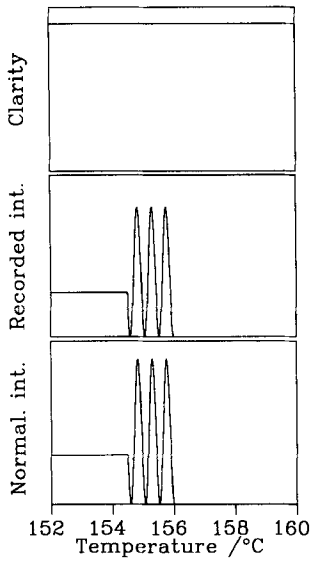

FIGURE 4 The idealised transition of Figure 1, as it would be recorded by the apparatus in Figure 2, showing clarity (top), recorded interference intensity (middle), and normalised interference intensity (bottom).

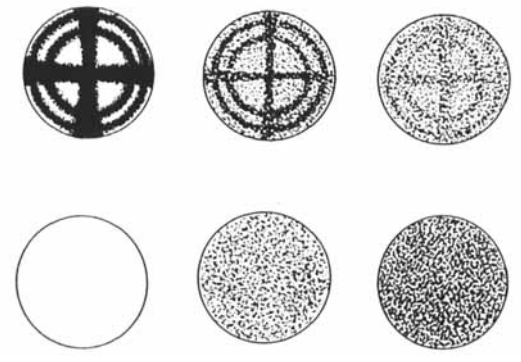

FIGURE 5 Representations of conoscopic images showing the effect of increased scattering (left to right), between crossed polars (top row) and without the analyser (bottom row).

The sample becomes opaque on passing through the isotropic-smectic transition as a result of scattering by the polydomain texture, although defects, a biphasic texture and thermal fluctuations may all contribute. The result is a loss of contrast in the conoscopic image, as depicted in Figure 5.

Before moving to an account of optical measurements it is important to note that an undulation in the clarity curve in the isotropic phase can arise as a result of thermal expansion in the sample which moves the glass slides, causing interference fringes from surface reflections. Figure 6 shows this effect, recorded with the beam passing through a part of the slide where there was no polymer present.

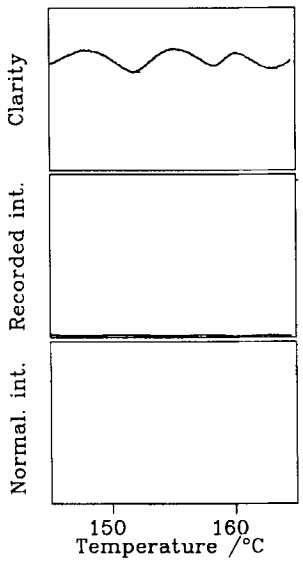

FIGURE 6 Control experiment, showing oscillation of transmitted light intensity due to interference between the rays reflected from the glass surfaces. The beam passes through a part of the slide where no polymer is present.

RESULTS AND DISCUSSION

AC Alignment: Effect of Different Voltages

Figure 7 shows the clarity, recorded and normalised interference intensity on cooling a 178 μm thick sample through the transition in fields of 400, 600 and 800 V. With a voltage below the alignment threshold (e.g. 400 V in this case), the usual polydomain texture develops, causing a sudden drop in clarity. There may be a brief rise in the recorded interference intensity due to developing birefringent domains, but it is masked by scattering which reduces the light intensity to levels which are too low to be reliably measured. Consequently, the normalised interference intensity gives random results.

With stronger fields (e.g. 600 and 800 V), the clarity falls at the transition, due perhaps to a biphasic region, and then rises slowly to a stable value which is higher for stronger fields. The normalised interference intensity (which is a better guide to the alignment than the recorded interference intensity) rises sharply at the transition, then oscillates for the next 1.5°C or so due to interference fringes, falls, and then rises slowly to a stable value. The behaviour is reversible on reheating with or without a field applied. These effects are therefore not due to backbone relaxation processes, which would not be reversible, and are likely to be due to the presence of a biphasic region which extends over about 5°C. The full width of the biphasic region is not detected by DSC, as will be shown.

It has previously been observed[29] that higher voltages, higher frequencies, and slower cooling rates produce clearer textures; we would expect the same conditions to produce better alignment. Experiments with a thin sample (30 μm) support this

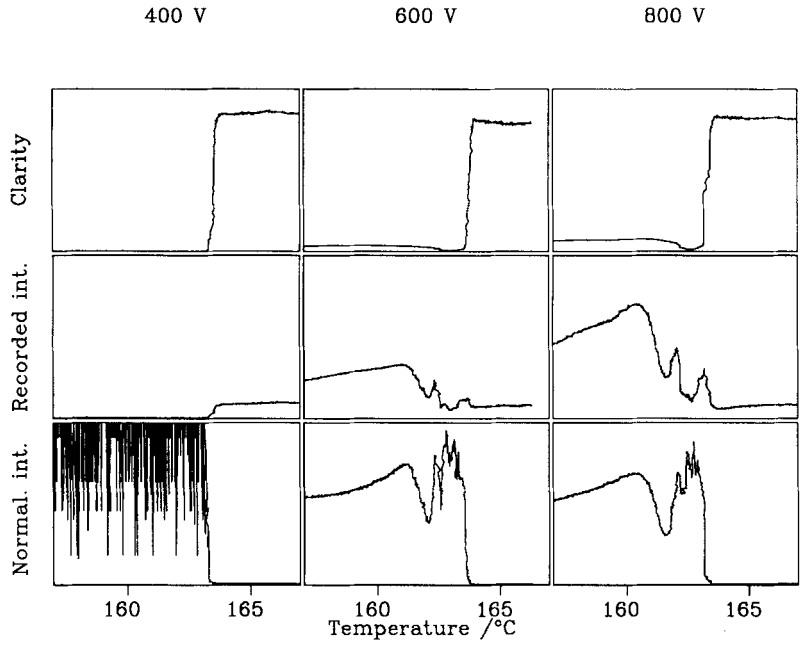

FIGURE 7 Experimental result from a thick sample, cooled with 400 V (left column), 600 V (centre), 800 V (right column) applied. Sample 178 μm thick, 3.33 kHz field, cooling at 1°C/min.

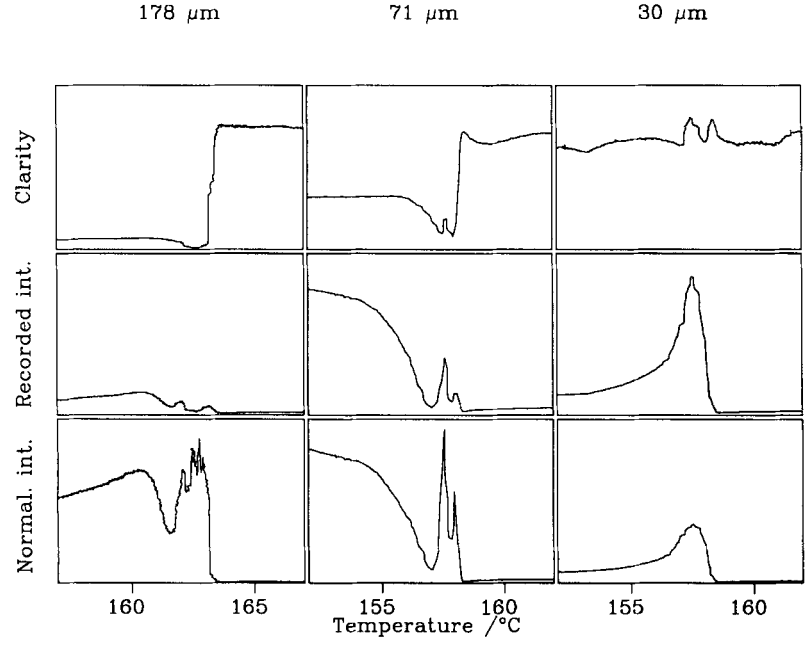

FIGURE 8 Number of interference fringes plotted against sample thickness.

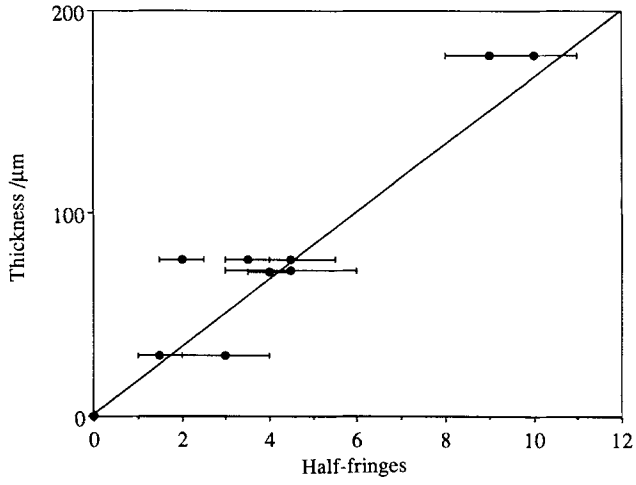

FIGURE 9 Interference fringes observed while cooling samples of various thicknesses in strong fields. 178 μm (left column), 71 μm (centre), 30 μm (right column).

prediction. At a low voltage the normalised interference intensity barely rises before polydomain scattering develops; at a slightly higher voltage the first interference fringe just starts to develop; at the highest voltage the first interference ring is well enough developed to cause a large reduction in the normalised interference intensity.

AC Alignment: Effect of Sample Thickness

It is important to remember that an increase in alignment causes the movement of fringes, and that simply obtaining a high value for the normalised interference intensity may imply poor alignment rather than good alignment. Thus a thick sample will show more fringes than a thin one (Figure 8), because the path difference between the ordinary and extraordinary rays is proportional to the thickness as well as the birefringence; the fringes will also be of lower contrast because of the greater scattering associated with the larger thickness.

In Figure 9 the sample thickness is plotted against the number of fringes observed to estimate the birefringence of the well-aligned material. The gradient of the line of best fit is 18.7 μm/half-wavelength retardation. We are observing the sample at an angle of 35°. If we assume that the refractive index of the polymer is about 1.6, then from Snell's Law the ray passes through the sample at $\theta = 21°$ to the normal. Since the observed birefringence for a one wavelength retardation is given by $\Delta n = \lambda_0 \cos\theta/d$, where λ_0 is the wavelength in a vacuum and d is the sample thickness, the observed birefringence is 0.016. The cross-section of a uniaxial indicatrix is an ellipse, so $(x/o)^2 + (y/e)^2 = 1$, where e and o are the extraordinary and ordinary refractive indices, which can also be written

$$\left(\frac{e' \cos\theta}{o}\right)^2 + \left(\frac{e' \sin\theta}{e}\right)^2 = 1$$

Inserting $o = 1.6$, $e' - o = 0.016$, $\theta = 21°$ we find that the birefringence of the material $e - o = 0.14$. Previous experiments[29] estimated the birefringence as 0.1.

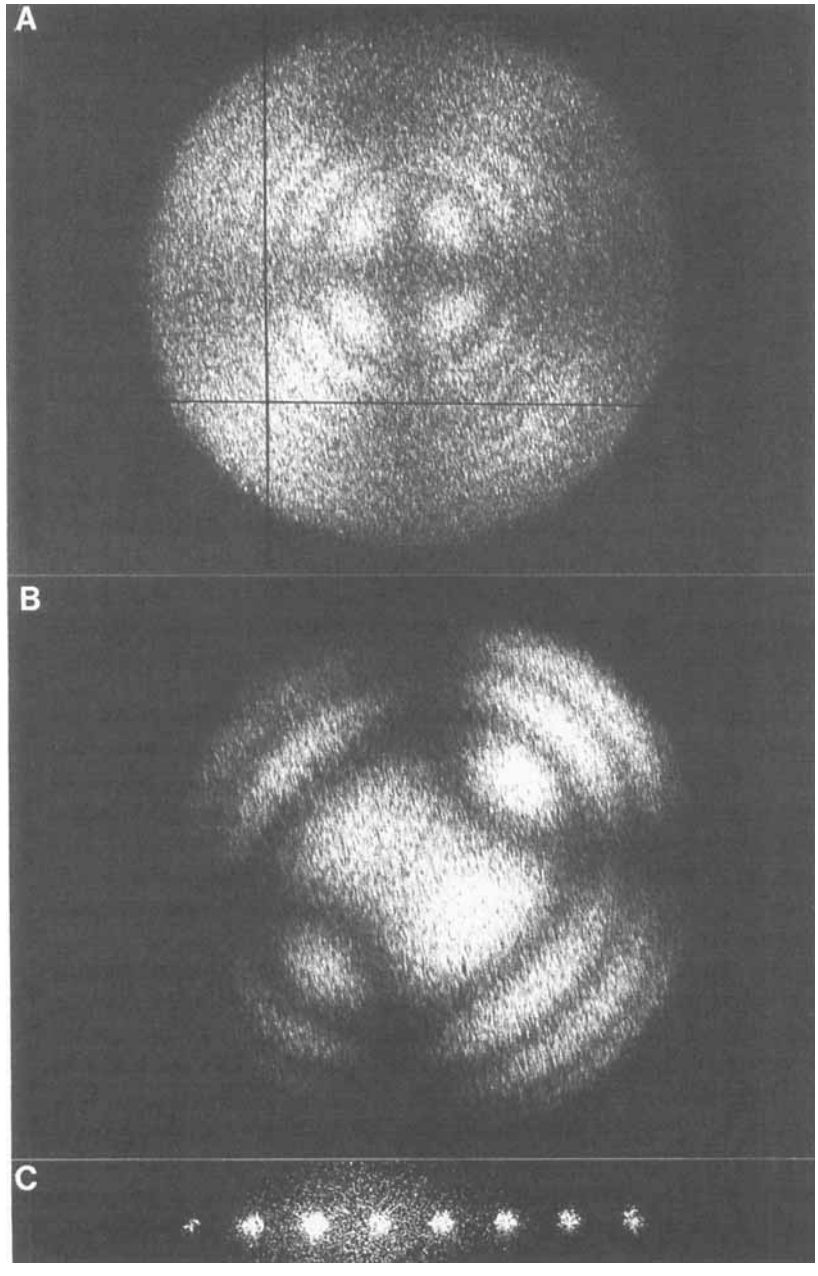

FIGURE 10 (a) Conoscopic image of the sample of Figure 13 in HeNe light. (b) Conoscopic image of aragonite. (c) Diffraction pattern from a grating with 300 lines/mm, photographed in the back focal plane.

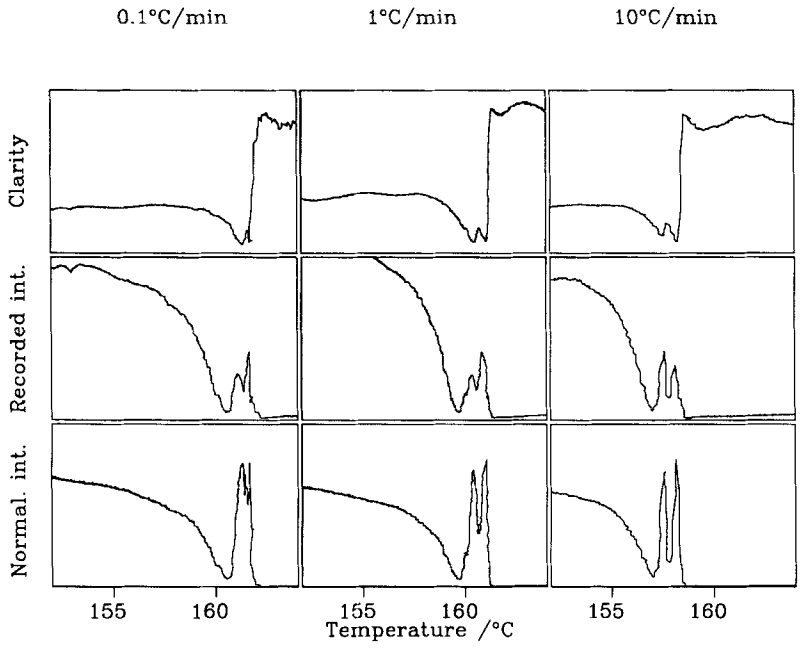

FIGURE 11 Cooling at different rates. 0.1°C/min (left column), 1°C/min (centre), 10°C/min (right column). 85 μm sample, 800 V, 3.33 kHz.

A careful direct comparison was made between the number of fringes observed while cooling and the number of rings seen on the conoscopic image after cooling. A sample was cooled at 1°C/min in a strong (800 V) electric field, and held 5°C below the transition for one hour (to improve the quality of the sample for conoscopy). Experiments in this temperature range indicate that the degree of alignment does not continue to change at these lower temperatures (see below). For the particular sample thickness chosen, both as recorded and normalised curves showed two peaks on cooling.

Figure 10a shows the conoscopic image of the same sample, photographed after cooling to room temperature, with the sample illuminated in HeNe laser light (as used in the optical technique). This conoscopic image was calibrated in two ways. First, the conoscopic image of aragonite in Figure 10b was photographed, under the same conditions as that of the sample. Aragonite is biaxial, with a melatope separation of $2V_\gamma = 18°$. After correcting for refraction at the top surface, this separation is 30° in air.[30] Second, the diffraction pattern in Figure 10c was photographed in the back focal plane, with the microscope objective focussed on a scratch on the ruled surface of a diffraction grating with 300 lines/mm. It is easy to confirm that the two methods of calibration are in precise agreement.

The beam passes through the poly(MO6ONS) sample in the optical experiment at 35° to the normal (in air), which is the same angle as the third-order peak on the diffraction pattern. It is now possible to mark the 35° position on Figure 10a, which is the part of the conoscopic image sampled by the optical technique (marked with a cross). Conoscopy therefore predicts that we should see four intensity max-

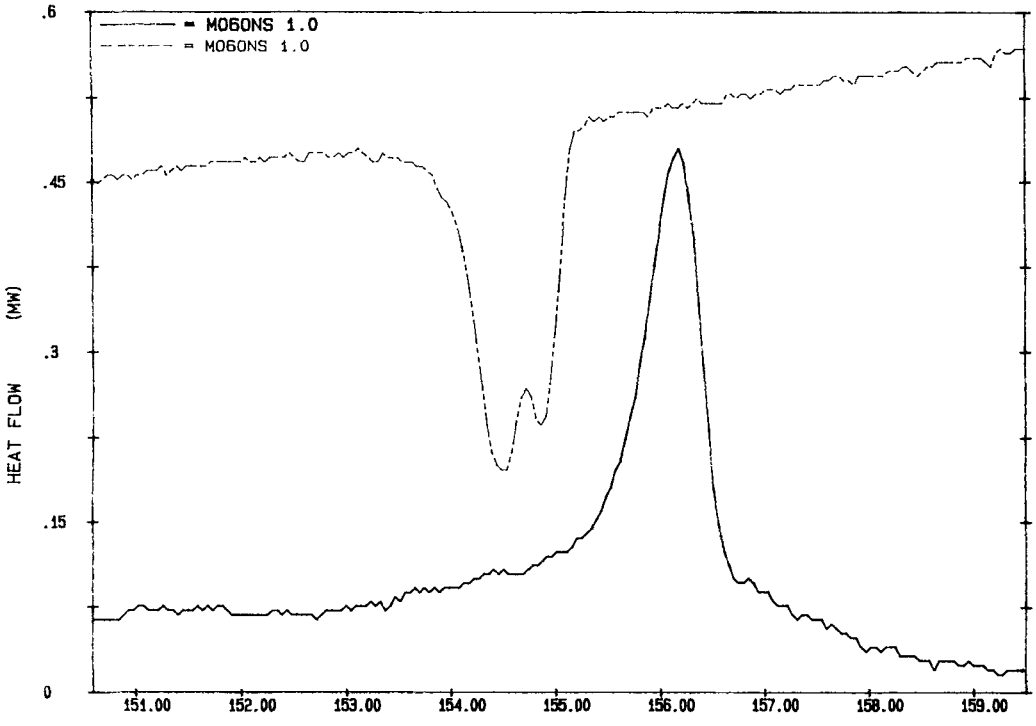

FIGURE 12 Differential scanning calorimetry of the unaligned material. Top curve: cooling. Bottom curve: heating. 3.75 mg sample, 2°C/min.

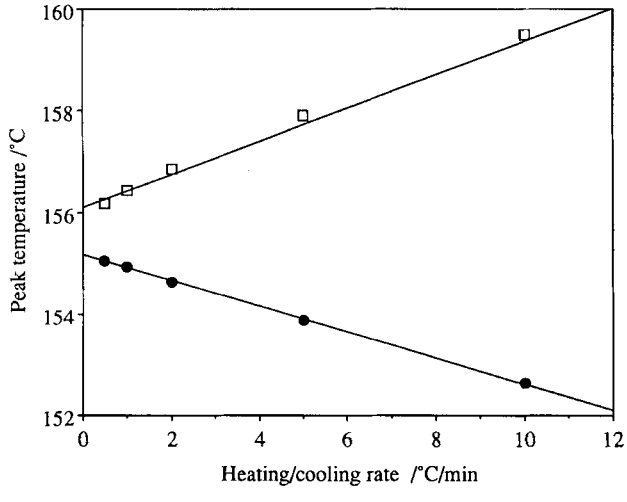

FIGURE 13 Peak positions determined by DSC plotted against heating/cooling rate. 11.95 mg sample (N.B. not the same sample as in Figure 17).

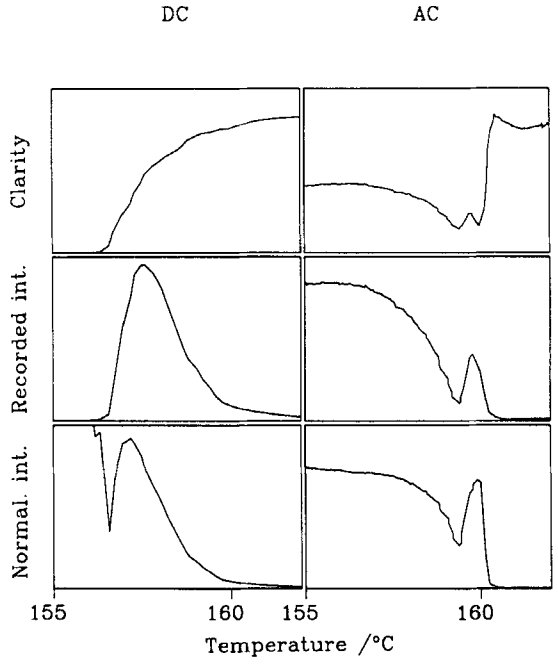

FIGURE 14 The different effects of a.c. and d.c. fields. Left: 800 V d.c. field, 76 μm sample. Right: 800 V peak-peak a.c. field at 3.33 kHz, 71 μm sample.

ima on the normalised interference curve, with the intensity stabilising well after the last peak.

However, the intensity curves (similar to those of the 71 μm sample of Figure 8) showed two peaks, whereas the conoscopic image would lead us to expect four. There is a suggestion of some earlier fringes when the normalised birefringence rises initially; indeed, there are changes in the recorded interference intensity in these initial stages of alignment, which are obscured on the normalised interference intensity curve by the rapidly changing clarity. We would expect alignment to be more rapid at these higher temperatures, a prediction supported by the fact that the interference fringes are more closely spaced at higher temperatures in experiments on thick samples (see Figure 7), which could cause several peaks to be concealed. Nevertheless, it is clear that there is not good agreement between the fringes observed while cooling and those seen using conoscopy, and the optical technique should not be used for quantitative measurements of birefringence when light scattering is significant.

AC Alignment: Effect of Cooling Rate

Figure 11 shows the alignment behaviour over two decades of cooling rates, showing that the temperature interval of the transition is independent of cooling rate and thus of time. This confirms that slow backbone motions do not play a significant rôle in the alignment kinetics in this range of cooling rates. Similarly, there is no obvious variation in the temperature range of the transition with applied voltage

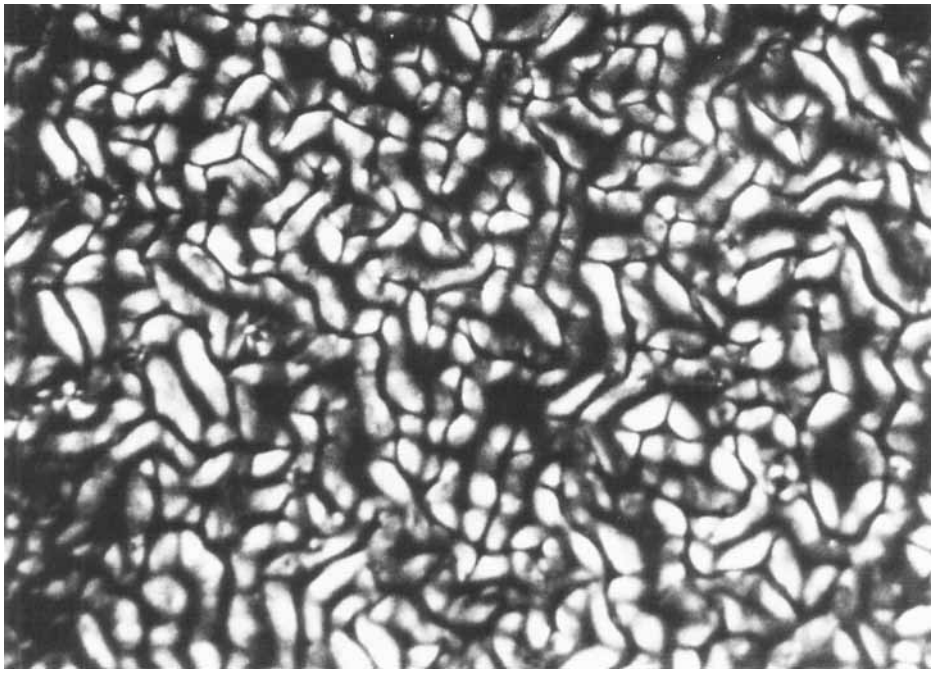

FIGURE 15 Photomicrograph of the electrohydrodynamic instability. White (tungsten) light, crossed polars, viewed normal to the sample, at a temperature just above the clearing point.

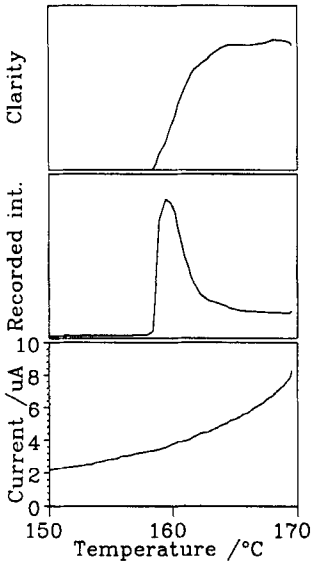

FIGURE 16 Cooling while monitoring current (bottom curve), showing that no change in conductivity behaviour occurs at the transition temperature. 71 μm sample, 1000 V d.c., 3°C/min.

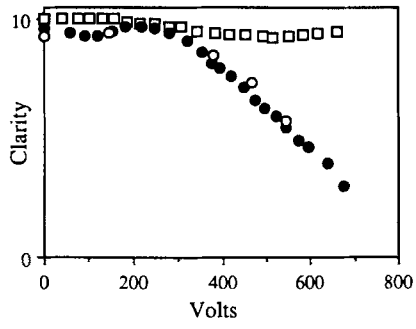

FIGURE 17 Dependence of clarity on d.c. voltage at two different temperatures above the transition temperature T_{cl}. Top curve: T_{cl} + 6.5°C; bottom curve: T_{cl} + 1.0°C (closed circles are on increasing the voltage, open circles are on reducing voltage, to show reversibility). 71 μm sample.

or frequency. The temperature interval is a little wider with thick samples (Figure 8), but that is probably due to temperature variations across the sample thickness.

Thermal Analysis

A careful study with a differential scanning calorimeter (Perkin-Elmer DSC7), using a low mass sample and slow heating and cooling rates, revealed that there is a double transition peak on cooling, but only a single peak on heating (Figure 12). It is possible that this effect is associated with a transient phase, although this has not been observed in the optical microscope. The full width of the biphasic region, as found using the optical technique, is neither seen here nor with heavier samples.

Peak positions were measured at various heating and cooling rates and extrapolated to zero (Figure 13), showing that the transition peak occurs at 156.1°C on heating and 155.2°C on cooling, showing supercooling. (It was not possible to correlate the DSC temperatures accurately with the transition temperatures observed optically, because the systematic error in the temperature control varies between samples in the optical experiments). This double peak is not understood, although the supercooling suggests that it may be due to different nucleation rates between the surfaces and the centre of the sample.

DC Electric Fields: Experimental

Figure 14 shows a comparison between the effect of a d.c. field and an a.c. field on the optical clarity and interference intensity on cooling at 10°C/min. There are two significant differences. Firstly, the d.c. field does not lead to a clear smectic monodomain on cooling through the transition, although there is a rapid rise in birefringence before it is swamped by increasing opacity. Secondly, the d.c. field causes a definite pretransitional effect. Note that the clarity gradually decreases on cooling over the range of about 5°C above the transition itself, while the birefringence (interference intensity) increases. No such pretransitional effects are apparent in a.c. fields.

Microscopy (Figure 15) reveals that the pretransitional scattering is due to

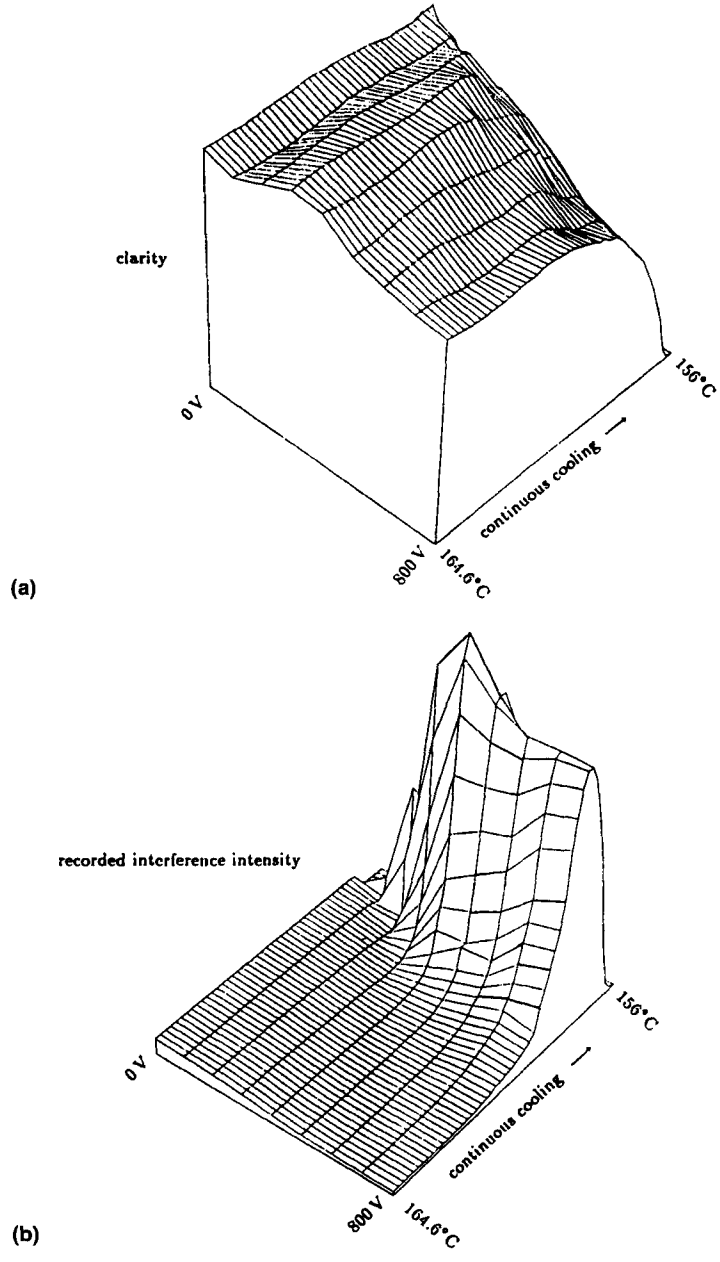

FIGURE 18 Cooling curves in d.c. fields of various strengths. 76 μm thick sample, 10°C/min.

electrohydrodynamic instability, shown as stirring in the material. One possible cause is isotropic mode charge injection, but this is thought not to be the case. The current passed by the sample showed a steady decline (Figure 16) during the experiment (as it does if held at constant temperature), with no change in behaviour at the transition temperature. In addition, the scattering is only seen if the voltage

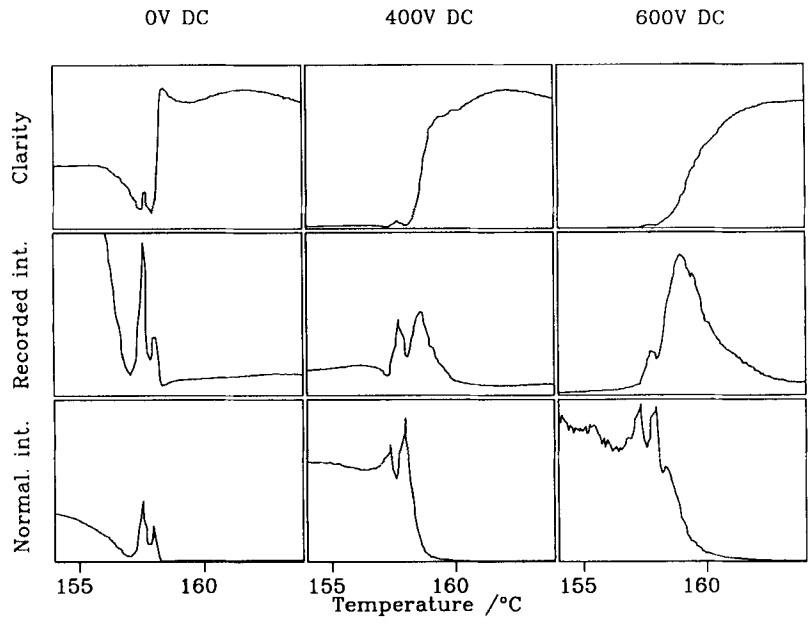

FIGURE 19 Simultaneous application of a.c. and d.c. fields on cooling. From left, d.c. voltages are 0, 400, 600 V. 71 μm sample, 800 V peak-peak a.c. field at 5 kHz, 3°C/min.

is applied near the transition temperature (Figure 17), whereas isotropic mode scattering, which is independent of liquid crystallinity, would also occur at higher temperatures. The instability is therefore considered to be an anisotropic mode which does not appear to fit the classification scheme described by Blinov *et al.*[26]

Figure 18 illustrates that the magnitude of the pretransitional effect on cooling (shown both as clarity in Figure 18a and as recorded interference intensity in Figure 18b) increases with increasing field strength. The pretransitional effect is much less marked on heating which may be because the instability needs time to develop, a process which may happen faster at higher temperatures where the viscosity is lower.

Experiments using d.c. fields on their own are of limited value, as the sample becomes opaque at the transition temperature, making any further effects undetectable. If an a.c. field is applied instead, then a clear texture is produced; a.c. and d.c. fields were therefore applied simultaneously to investigate the effect of d.c. fields below the clearing point (Figure 19). The scattering produced by the d.c. field appears above the transition as usual, causing some pretransitional alignment, although this is weaker than the alignment caused by a.c. fields alone. Below the transition, the behaviour broadly seems to be the same as in a.c. fields only, but with a reduction in clarity and an increase in the normalised interference intensity due to the instability textures caused by the d.c. field, which disalign the smectic domains.

The d.c. field does have a small poling effect. The Pockels coefficient for a 71 μm sample cooled in 800 V pk-pk 5 kHz and 400 V d.c. was $r_{33} - r_{13} \sim 70$ fm V^{-1}. This is about 300 times less than for lithium niobate.[31]

DC Electric Fields: Influence of Molecular Design

The side group was designed expressly for NLO applications, and therefore has a strong permanent dipole as well as a large dielectric anisotropy. The dipole makes the side group susceptible to d.c. fields, enhancing the likelihood of pretransitional instabilities. The absence or weakness of pretransitional effects in a.c. fields is surprising, but may be explained in two ways. It is known empirically that instabilities are strongly frequency dependent, and it may be that the threshold field is very high in the range of a.c. frequencies used. On a molecular level, it may be that the side groups are so mobile in the isotropic phase that there is insufficient anisotropic behaviour to allow significant quadrupolar alignment by the field; they may only align once the smectic phase starts to nucleate, when the side groups are anchored into the interdigitated structure by the smectic field, as the nuclei then have a larger dielectric anisotropy than the individual side groups. This is supported by the observation of Zentel *et al.*[32] that the onset of the δ-relaxation process in a side chain liquid crystalline polymer with a methacrylate backbone coincided with the upper limit of the smectic phase.

d.c. fields become ineffective as soon as the interdigitated structure forms, as the smectic nuclei have no net dipole moment (but they can still be aligned by a.c. fields because of their strong net dielectric (quadrupolar) anisotropy). Thus the design of the molecule and the consequential interdigitated structure oppose polar alignment, and a redesign of the molecule is needed before materials which can form very high $\chi^{(2)}$ structures can be synthesised.

In addition, the instability encourages a scattering texture to form (which is undesirable in optical devices) and decreases the polar alignment of the material. The material also degrades in d.c. fields, possibly due to a limited amount of electrochemical reaction at the surfaces. These are well known problems with d.c. fields, and are the reasons that poling is usually performed close to the glass transition. Kozak *et al.*[27] have reported some success with d.c. alignment at constant temperature in the nematic phase of a side chain liquid crystalling polymer, but the maximum alignment was only $S = 0.25$, and they acknowledge that instabilities may cause this poor alignment.

CONCLUSIONS

The novel method for monitoring alignment performs well while sample clarity is reasonably good, providing results which are useful qualitatively, but which are of limited quantitative value with the present materials because of light scattering. An example was given where the optical method was more sensitive to a continued phase change than DSC.

On cooling in a uniform alternating electric field, poly(MO6ONS) shows no pretransitional alignment, but there is an interval of about 5°C (independent of the cooling rate) below the clearing point during which the material aligns. The alignment is reversible on reheating with or without an electric field, which is evidence for a biphasic region, and illustrates the limited influence of backbone relaxation processes. Stronger fields produce more strongly aligned samples, but above the

threshold field (which is dependent on the sample thickness and cooling rate) little extra alignment is gained by increasing the field strength.

On cooling from the isotropic to the smectic phase with a d.c. field applied, electrohydrodynamic instabilities appear above the transition temperature and a scattering texture develops. Application of a.c. electric fields under the same conditions usually produces transparent, well aligned monodomains once the smectic phase begins to appear, but no pretransitional effects have been seen. Simultaneous application of a.c. and d.c. fields lends to some reduction of the instabilities and resulting scattering textures, and the resulting sample has a small non-linear optical coefficient, showing that some poling has occurred. The major limitation to the effectiveness of d.c. poling of these polymers is connected with the interdigitated structure of the smectic A phase, and the tendency to interdigitate must be reduced in future materials if good, stable poling is to be achieved.

Acknowledgment

We would like to thank Hoechst-Celanese for funding and for much support, and particularly Tony East for synthesising the materials, and Ilmar Kalnin for electro-optic expertise; also the Science and Engineering Research Council, and Lt. Col. Chester Dymek of the US Air Force Office of Scientific Research for funding. We are indebted to Keith Page in our department for electronics support.

References

1. C. Tani, *Appl. Phys. Lett.*, **19**, 241–242 (1971).
2. D. Coates, W. A. Crossland, J. H. Morrissy and B. Needham, *J. Phys. D: Appl. Phys.*, **11**, 2025–2034 (1978).
3. J. A. M. M. van Haaren and G. L. J. A. Rikken, *Phys. Rev. A*, **40**, 5476–5479 (1989).
4. M. Hareng, S. Le Berre and L. Thirant, *Appl. Phys. Lett.*, **25**, 683–685 (1974).
5. D. K. Rout and R. N. P. Choudhary, *Mol. Cryst. Liq. Cryst.*, **166**, 75–90 (1989).
6. H. J. Coles and R. Simon, *Recent Advances in Liquid Crystal Polymers*, (ed. L. L. Chapoy). Elsevier Applied Science Publishers, 1985, pp. 323–334.
7. R. Simon and H. J. Coles, *Mol. Cryst. Liq. Cryst.*, **102**, (Letters), 43–48 (1984).
8. R. Simon and H. J. Coles, *Polymer*, **27**, 811–816 (1986).
9. S. Ujie, N. Koide and K. Iimura, *Mol. Cryst. Liq. Cryst.*, **153**, 191–198 (1987).
10. H. J. Coles and R. Simon, *Mol. Cryst. Liq. Cryst. Lett.*, **1**, 75–81 (1985).
11. H. J. Coles and R. Simon, *Mol. Cryst. Liq. Cryst.*, **102**, (Letters), 75–80 (1984).
12. M. Steers and A. Mircea-Roussel, *J. Physique Colloq.*, **37**, C3-145 (1976).
13. W. Haase and H. Pranoto, *Progr. Colloid & Polym. Sci.*, **69**, 139–144 (1984).
14. D. Coates, W. A. Crossland, J. H. Morrissy and B. Needham, *Mol. Cryst. Liq. Cryst.*, **41**, (Letters), 151–154 (1978).
15. W. Haase and D. Pötzsch, *Mol. Cryst. Liq. Cryst.*, **38**, 77–85 (1977).
16. H. Ringsdorf and R. Zentel, *Makromol. Chem.*, **183**, 1245–1256 (1982).
17. H. Pranoto and W. Haase, *Mol. Cryst. Liq. Cryst.*, **98**, 299–308 (1983).
18. A. Kozak, G. P. Simon and G. Williams, *Polymer Communications*, **30**, 102–105 (1989).
19. G. S. Attard and G. Williams, *Polymer Communications*, **27**, 66–68 (1986).
20. G. S. Attard and G. Williams, *Polymer Communications*, **27**, 2–5 (1986).
21. J. H. Wendorff and M. Eich, *Mol. Cryst. Liq. Cryst.*, **169**, 133–166 (1989).
22. G. R. Möhlmann and C. P. J. M. van der Vorst, *Side Chain Liquid Crystalline Polymers*, edited by C. B. McArdle (Blackie, London, or Chapman and Hall, New York) Chapter 12.
23. R. Simon and H. J. Coles, *Liquid Crystals*, **1**, 281–286 (1986).
24. E. F. Carr, *Mol. Cryst. Liq. Cryst.*, **13**, 27–36 (1971).
25. M. Moheban, W. Montoya, R. Parker and D. Siden, Raychem Corp., Patent priority US 173407 (880325).

26. L. M. Blinov, M. I. Barnik and A. N. Trufanov, *Mol. Cryst. Liq. Cryst.*, **89**, 47 (1982).
27. A. Kozak, G. P. Simon and G. Williams, *Polymer Communications*, **30**, 102 (1989).
28. R. B. Findlay, T. J. Lemmon and A. H. Windle, *J. Mater. Res.*, **6**, 604–609 (1991).
29. R. B. Findlay and A. H. Windle, *Mol. Cryst. Liq. Cryst.*, **206**, 55–64 (1991).
30. C. Viney, private communication.
31. S. Martin, Cavendish Laboratory, University of Cambridge, private communication.
32. R. Zentel, G. R. Strobl and H. Ringsdorf, *Macromol.*, **18**, 960–965 (1985).